Atomization and Sprays, 26 (7): 673–686 (2016)

INTERNAL FLOW PHYSICS OF A FLUIDIC OSCILLATOR SPRAY IN THE TRANSITION REGIME

Mehmet N. Tomac[1] & James W. Gregory[2,*]

[1]*Department of Mechanical Engineering, Abdullah Gül University, 38080, Kayseri, Turkey*

[2]*Department of Mechanical and Aerospace Engineering, The Ohio State University, Columbus, OH 43210, USA*

[*]Address all correspondence to: James W. Gregory, E-mail: gregory.234@osu.edu

Original Manuscript Submitted: 12/08/2014; Final Draft Received: 06/10/2015

An experimental investigation of the underlying flow physics of a dual-jet interaction fluidic oscillator spray has been conducted in the transition regime for a Reynolds number of 1680. The transition regime is defined as a narrow range of flow rates between two other operating modes of the fluidic oscillator. Particle image velocimetry (PIV) was used with refractive index–matching sodium iodide solution to minimize reflections from the spray geometry and obtain detailed internal velocity fields. PIV results show that the interaction of the two internal jets and the resultant vortices are responsible for the oscillation mechanism in the transition regime. Two side vortices sustain their existence throughout the oscillation period by altering their size, shape, and strength, and a dome vortex is created twice each oscillation period (once from each jet). The dome vortex plays a key role in the kinetic energy transfer mechanism inside the oscillator by means of jet bifurcations. The primary oscillation mechanism in the transition regime is that each internal jet's connection with the exiting jet is cut completely by the dome vortex in every period. This is in contrast to the low–flow rate oscillation mechanism, in which the oscillations are created by continuous collisions of the jets. Furthermore, the internal jets are observed to energize the side vortex on the opposite side of the chamber—a phenomenon that was not observed in the low–flow rate regime.

KEY WORDS: *sprays, fluidic oscillators, jet interactions, transition regime*

1. INTRODUCTION

Fluidic oscillators are devices that create an unsteady oscillating jet with variable frequency that depends primarily on the supplied flow rate (or pressure). These mechanically simple devices have no moving parts, making them attractive for applications such as spray nozzles and unsteady injectors. Both the high-frequency unsteadiness and the distributed nature of the fluidic oscillator jet (Fig. 1) are particularly important for spray applications.

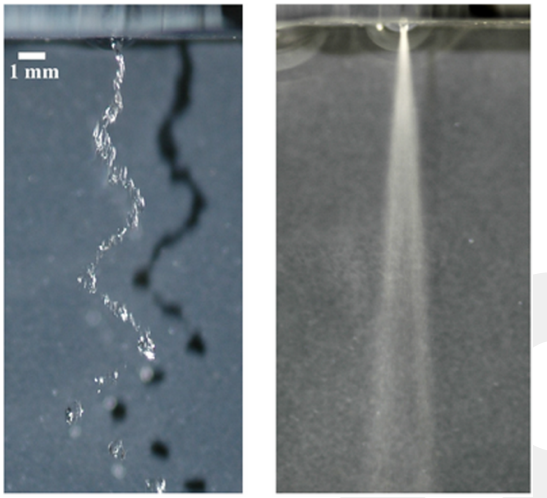

FIG. 1: Water visualizations of a microscale fluidic oscillator flow field illustrating the spray pattern: (left) instantaneous and (right) time averaged (from Gregory et al., 2007).

Characterization of the internal and external fluid dynamics of fluidic oscillators has become important since different spray and injector applications require a comprehensive understanding of the oscillation mechanisms for thoughtful implementation. Although the most common way to create a spray is the spray nozzle, other methods, such as pressure, centrifugal, electrostatic, and ultrasonic, are also used. However, fluidic oscillators are quite different than the other spray devices due to their superior properties, such as high control authority, wide range of operating frequencies, distributed nature of momentum addition, simplicity, lack of moving parts, and ability to generate an unsteady sweeping jet with sinusoidal, square, and sawtooth (Raman et al., 1999) wave patterns, as reviewed by Raghu (2013) and Gregory and Tomac (2013). Fluidic oscillator sprays were studied in various combustion applications. Guyot et al. (2009) used fluidic oscillators for fuel flow modulation for a combustor. Recently, Bobusch et al. (2015) used a fluidic oscillator to obtain higher mixing quality, which leads to a higher combustion efficiency.

Fluidic oscillators can be classified in two main types. The first type is the wall attachment fluidic oscillator, which operates based on the Coanda effect and has been extensively studied since the fluidics era of the 1960s (e.g., Warren and Peperone, 1962; Booth, 1962; Spyropoulos, 1964; Lush, 1968; Gaylord and Carter, 1969; Tesař and Bandalusena, 2011; Bobusch et al., 2013; Tesař et al., 2013). However, this work studies a relatively new type of fluidic oscillator that is based on internal jet collisions and interactions. The collision of opposed jets has been known to yield self-sustained oscillations (Nomoto et al., 1972; Denshchikov et al., 1978, 1983; Rolon et al., 1991; Pawlowski et al., 2006; Hassaballa and Ziada, 2015) if certain parameters, such as the distance between nozzles and the characteristic jet velocity, are selected properly. One of the early

fluidic oscillators based on internal jet interactions is the so-called "feedback-free" fluidic oscillator developed by Raghu (2001). This oscillator creates self-sustained oscillations based on the collision of two inclined jets in a dome-shaped mixing chamber. The geometrical outline of this fluidic oscillator can be seen in Fig. 2.

Gregory et al. (2005) investigated the internal jet interactions of the feedback-free fluidic oscillator by using pressure-sensitive paint and concluded that an unsteady shear layer that is driven by two counterrotating side vortices governs the oscillation process. In another study, Gregory et al. (2007) used a microscale version of the feedback-free fluidic oscillator to determine the oscillator's external flow characteristics. They reported that the variation of frequency with flow rate is linear, but with a discontinuity in slope at a particular flow rate that was indicative of a change in oscillation modes. In their combined experimental and numerical study, Bidadi et al. (2011) discussed how the unstable arrangement of the jet interaction creates vortices that eventually dictate the oscillatory behavior. In another study, Meier and Heister (2014) studied the jet interaction fluidic oscillator numerically for various flow conditions and oscillator geometries to use them to increase the mixing and combustion control ability in combustion applications. They were able to correlate the frequency characteristics of the oscillator with 2-D computational fluid dynamics (CFD) analysis, although 2-D analyses were previously reported to be 50% lower than the actual frequency provided by the oscillator (Tomac, 2013). In a preliminary study, Tomac and Gregory (2012) used particle image velocimetry (PIV) to measure the dual-jet interactions in the interaction chamber of a feedback-free fluidic oscillator. They determined the existence of three distinct flow regimes and suggested that there were different oscillation mechanisms depending on the flow rate (Reynolds number). The low–flow rate and transition–flow rate regimes were observed for very low *Re*, while the high–flow rate regime constituted the normal operating range for that particular scale of fluidic oscillator. The low–flow rate behavior was discussed in detail by Tomac and Gregory (2013, 2014). They concluded that the two jets collide with each other continuously and that neither of the jets is completely cut by the dome vortex that governs the bifurcation and the kinetic energy transfer process between the two jets.

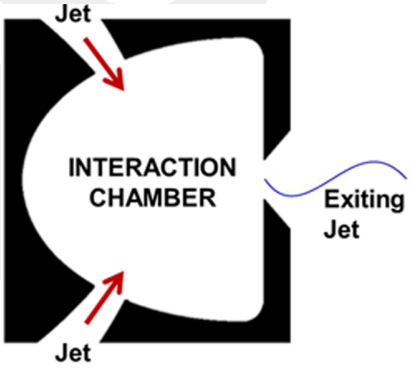

FIG. 2: Feedback-free fluidic oscillator design of Raghu (2001).

The transition regime is defined as a narrow range of flow rates between the other two regimes, representing a distinct operating mode from the other two. The present study focuses on the details of the jet interactions and oscillation mechanism of the feedback-free fluidic oscillators in the transition regime by using a refractive index–matched PIV technique. This investigation aims to understand the detailed flow physics of dual-jet interactions, jet bifurcations, jet cutoff, kinetic energy transfer mechanisms, vortex–shear layer and vortex–wall interactions, and the overall oscillation mechanism of the feedback-free fluidic oscillator in the transition regime.

2. EXPERIMENTS

The internal flow field of the feedback-free fluidic oscillator was extracted with the help of refractive index–matched PIV technique together with a custom microphone-tube sensor configuration and a quarter period–based PIV phase-averaging method. The details of this experimental setup are described in the following.

2.1 Fluidic Oscillator Model

The fluidic oscillator model used for this investigation was 12.5 mm in width, 15 mm in length, and 1.5 mm in depth. The nozzle width of both internal jets was 1.70 mm, and the exit nozzle width was 2 mm. The models were fabricated from clear acrylic by laser cutting three parts. These parts were stacked to form the oscillator assembly and secured with acrylic glue. Dimensions of the fluidic oscillator and the three parts' design are shown in Fig. 3. In this figure, the angle of an internal jet with respect to the

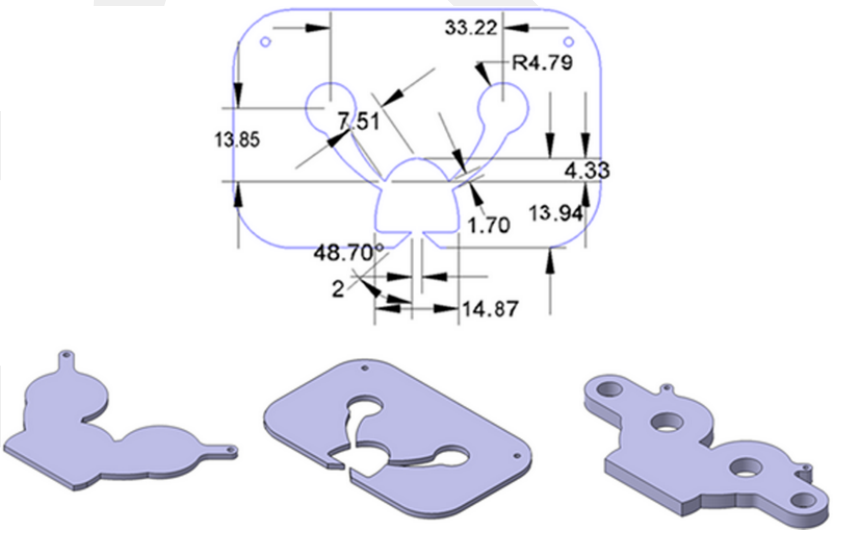

FIG. 3: Dimensions of the fluidic oscillator in millimeters (depth is 1.5 mm) and (bottom) the isometric view of the three parts.

symmetry line of the interaction chamber is 32°. Primary concerns for the fabrication of the oscillator were optical access, geometrical precision, and prevention of any leaks.

2.2 Refractive Index–Matched PIV Technique

PIV was selected to measure the phase-averaged internal flow field resulting from the jet interactions. However, reflections of laser light energy from acrylic–air or acrylic–water interfaces due to differences in the refractive index will significantly diminish the quality of the experimental data. To prevent these reflections, a refractive index–matched fluid of sodium iodide (NaI) solution was used. The prepared solution consisted of 60% NaI by weight with a density of 1730 kg/m^3 and a volume of 5 L. Hollow glass spheres were used for seeding, and density differences between the seed and fluid were found to produce negligible buoyancy-induced velocity errors. A schematic of the experimental setup is shown in Fig. 4: a 200 mJ double-pulsed Nd:YAG 532 nm laser (New Wave Solo XT 200) with sheet-forming optics (spherical and cylindrical lens), a programmable timing unit (LaVison External PTU V. 9.0), and a charge-coupled device (CCD) camera (PCO 1600) with a macrolens (Sigma 105 mm, 1:2.8D) were used. The time separation between two laser illuminations was 300 μs, and LaVision's Davis software was used for data acquisition and postprocessing, in conjunction with LabView 8.6 and MATLAB R2011b.

The flow rate through the oscillator was measured with a flow meter (Omega Engineering FLR1011ST) that was specifically calibrated for the refractive index–matching fluid. The synchronization signal for phase averaging was obtained through a microphone-tube sensor configuration that operated based on a condenser microphone. Small fluctuations in the flow rate complicated the phase-averaging process, precluding any in situ phase-locking efforts. To solve this problem, a quarter period–based PIV

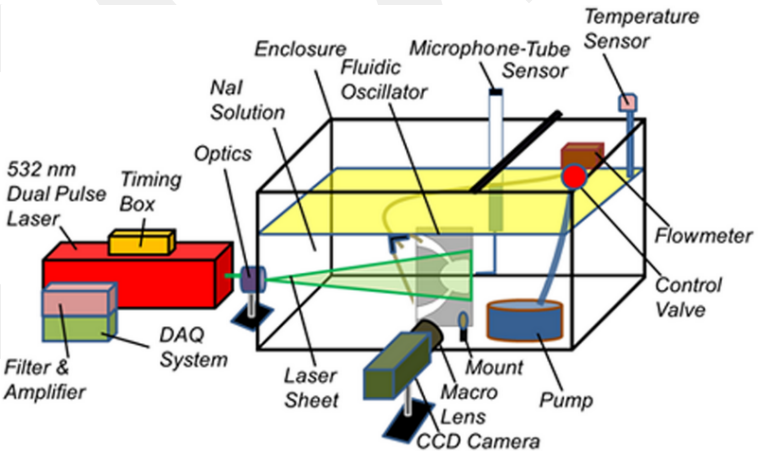

FIG. 4: Schematic of the experimental setup.

phase-averaging method was used [the details and the entire experimental setup of which are discussed by Tomac and Gregory (2014)].

Six hundred images were acquired for the flow rate presented in this article, and the period of the oscillation, as shown in Fig. 5, was divided into 40 phases. Each bin covers a phase angle range of 9°, and the images that fell into the same bin were averaged. The maximum number of images in each phase bin was 18, and the minimum number of images was 11. The oscillation frequency for the flow rate presented in this work was 26.5 Hz, with an average period of 37.7 ms. The Reynolds number was calculated based on the exit width, average velocity at the exit of the oscillator, and the kinematic viscosity of the NaI solution at 28.8°C.

3. RESULTS

Tomac and Gregory (2012) reported three distinct operating regimes across a range of flow rates from 2.8 to 15 mL/s, as shown in Fig. 6. The transition regime, spanning a narrow range of flow rates from 3.5 to 4.0 mL/s, yielded a plateau region in the flow rate–frequency plot at about 26.5 Hz. The results discussed in this section correspond to a flow rate of 3.5 mL/s (Re = 1680), as indicated by the arrow in Fig. 6. Tomac and Gregory (2014) investigated the internal flow field in the low–flow rate regime. They concluded that the oscillation mechanism in the low–flow rate regime is due to the continuous collision of two internal jets and that both jets feed the exiting jet (i.e., no jet is the sole supplier of the exiting jet). However, when the transition regime starts, the frequency decreases abruptly, and the transition regime reveals itself as a plateau region in the flow rate–frequency graph shown in Fig. 6. The current study distinguishes the

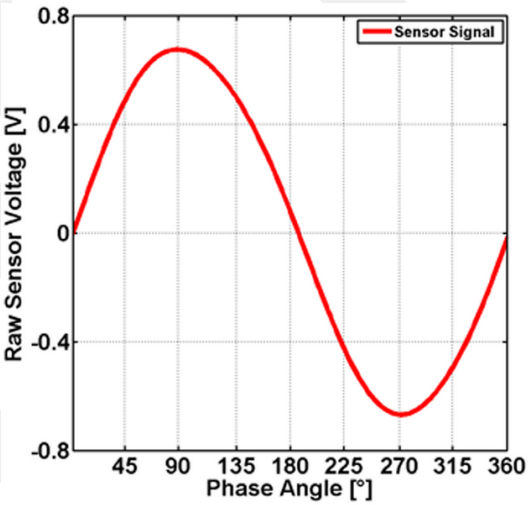

FIG. 5: Sample oscillation period for recorded microphone-tube sensor data showing the phase angle definitions.

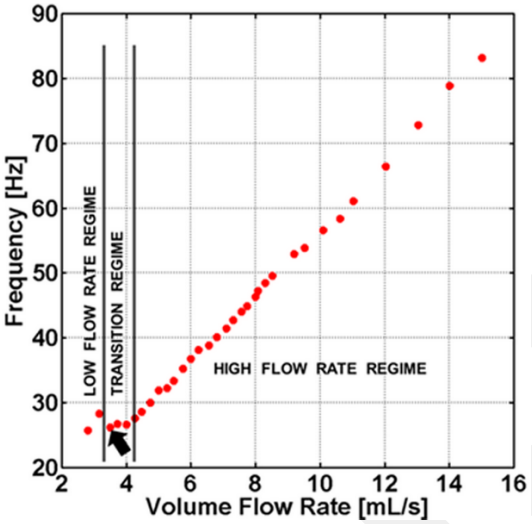

FIG. 6: Frequency characteristics of the fluidic oscillator.

transition regime from the low–flow rate regime even though the predominant oscillation mechanism was observed to be similar. The discussion presented here illuminates the unknown flow physics of dual-jet interactions and bifurcations, jet cutting and bending, the role of the side and dome vortices in the oscillation mechanism, and the interaction of the walls with the jets and the vortices in the transition regime.

For the purposes of identifying key features in the flow, Fig. 7 shows flow streamlines superimposed onto vorticity contours at one phase within the oscillation period. The two jets create four shear layers in total, two created by the upper jet (3–4) and two created by the lower jet (1–2). The upper-jet right shear layer (4) feeds the upper-side vortex

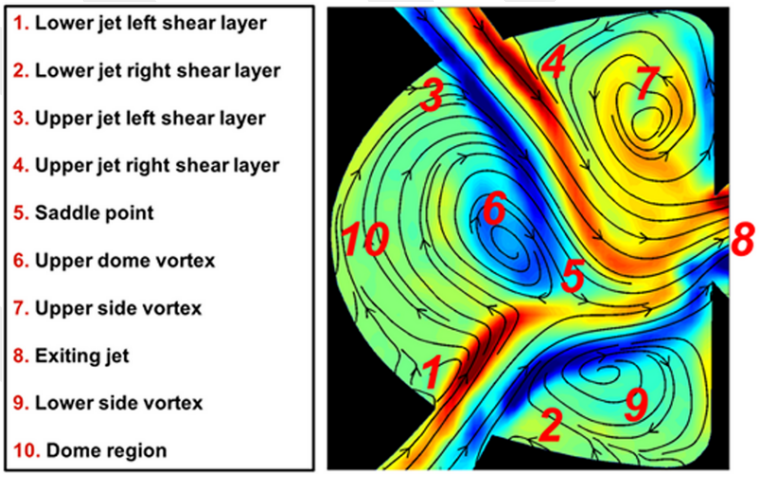

FIG. 7: Nomenclature for internal flow structures and regions.

(7), and the upper-jet left shear layer (3) feeds the upper-dome vortex (6). Likewise, the lower-jet right shear layer (2) feeds the lower-side vortex (9), and the lower-jet left shear layer (1) feeds the lower-dome vortex, which does not exist for this phase but forms in the other half-period of the oscillations. The dome vortices form and vanish depending on the phase; however, the side vortices persist with changing size, shape, and strength. The lower jet of the oscillator is bifurcated, as indicated by the saddle point at (5). The left branch of the bifurcated lower jet coalesces with the upper jet through the dome region (10). Eventually, owing to the interaction of all these flow structures, an unsteady oscillating exiting jet (8) is created at the exit of the fluidic oscillator.

Figure 8 shows the streamlines superimposed on the velocity (left) and vorticity (right) contours for 0° phase angle. For this phase angle, the main difference from the low–flow rate regime (Tomac and Gregory, 2014) can be easily observed. Unlike the low–flow rate regime, the lower jet's connection with the exiting jet is completely cut. Instead, it is bifurcated into two branches, neither of which is directly connected with the exiting jet at this instant. The left branch of the lower jet coalesces with the upper jet by transferring some of its kinetic energy to the upper jet. The right branch of the lower jet is forced toward the lower-side vortex region and is trapped in this region. The velocity of the lower jet is high enough such that the upper jet is substantially deflected. This deflection of the upper jet causes its potential core to directly energize the lower-side vortex. (This was not the case for the low–flow rate regime, where both jets collided along the oscillator's centerline and mutually fed the jet exit.) At this phase position, the potential core of the upper jet is moving toward the exiting jet to connect with it. The lower-side vortex pushes the lower jet toward the dome region, while a lower-dome vortex is forming and growing stronger as it constricts the left branch of the lower jet. Furthermore, as the lower-side vortex grows stronger, it increases the vorticity of the negative sign above the wall next to the exit orifice. At this phase, the upper-side vortex

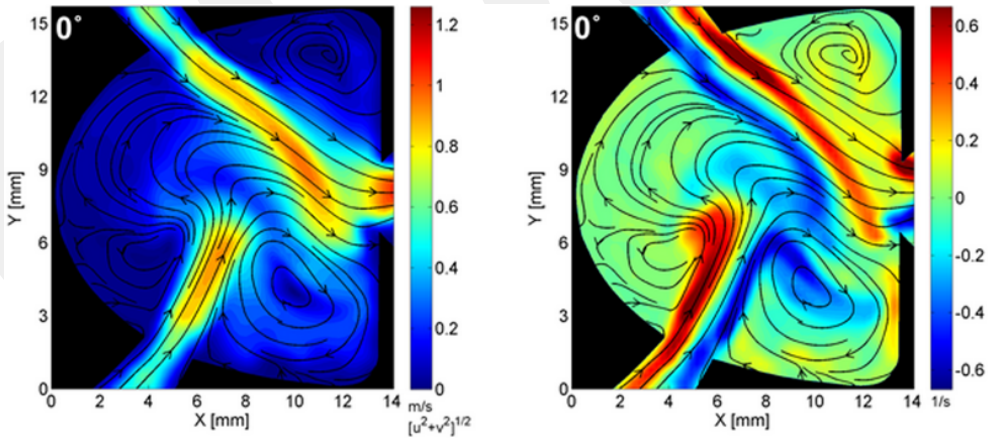

FIG. 8: Streamlines superimposed on (left) velocity and (right) vorticity contours at 0° phase angle in the transition regime.

is not energized by the upper-jet right shear layer, and the vorticity present is a remnant from earlier phases.

Figure 9 presents the results for a phase angle of 45°. As shown, the lower-dome vortex has moved toward the upper jet. As it grows, it pushes the lower jet toward the exiting jet and toward the lower-side vortex, while constricting the left branch of the lower jet, which is coalescing with the upper jet. Although the upper jet is about to cease energizing the lower-side vortex since the upper-jet core is entirely connected to the exiting jet, the lower-jet right shear layer continues to feed the lower-side vortex. Furthermore, as the strong lower-dome vortex is pushing the lower jet toward the exiting jet and the lower-side vortex, the vorticity in the sidewall boundary layer is significantly increased from the previous phase shown in Fig. 8.

At a phase angle of 90°, shown in Fig. 10, the lower-dome vortex has reached the upper jet and started bifurcating the upper jet. Owing to this bifurcation, the upper jet's left branch flows through the dome region, coalesces with the lower jet, and transfers some of its kinetic energy to the lower jet. The left branch of the upper jet also weakens as the lower-dome vortex bifurcates, increasing portions of the upper jet. At the same time, a small upper-dome vortex fed by the upper-jet left shear layer starts to form.

Figure 11 shows the final phase inside the interaction chamber of the fluidic oscillator in the transition regime before the upper jet is completely cut by the lower-dome vortex. At this instant, the upper jet left branch is coalescing with the lower jet, and its right branch is still connected with the exiting jet. The size and the strength of the lower-side vortex are decreased significantly, and it is not being energized by the lower-jet right shear layer any longer. Furthermore, the upper-jet right shear layer is being pushed toward the upper-side vortex region; however, it is not energizing the upper-side vortex since the jet is still connected with the exiting jet. Nevertheless, as the upper-jet right shear layer gets closer to the wall near the exit orifice, the vorticity in the wall boundary layer is increased slightly.

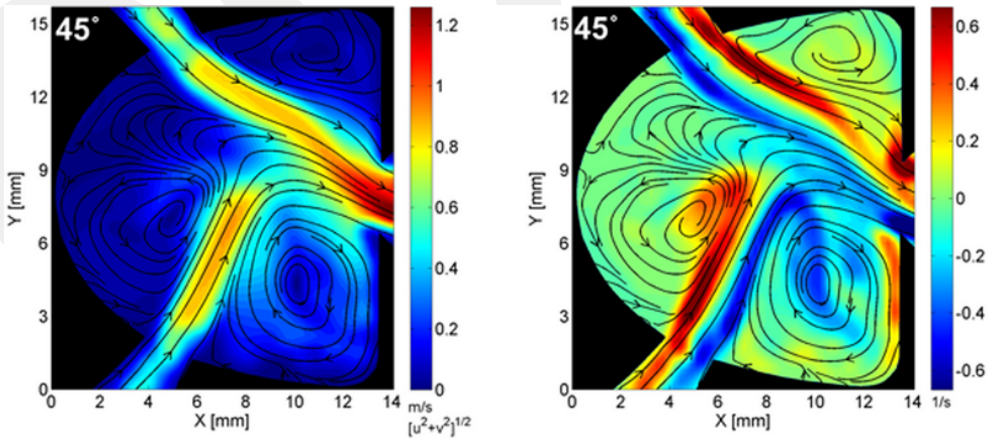

FIG. 9: Same as Fig. 8, but for 45° phase angle.

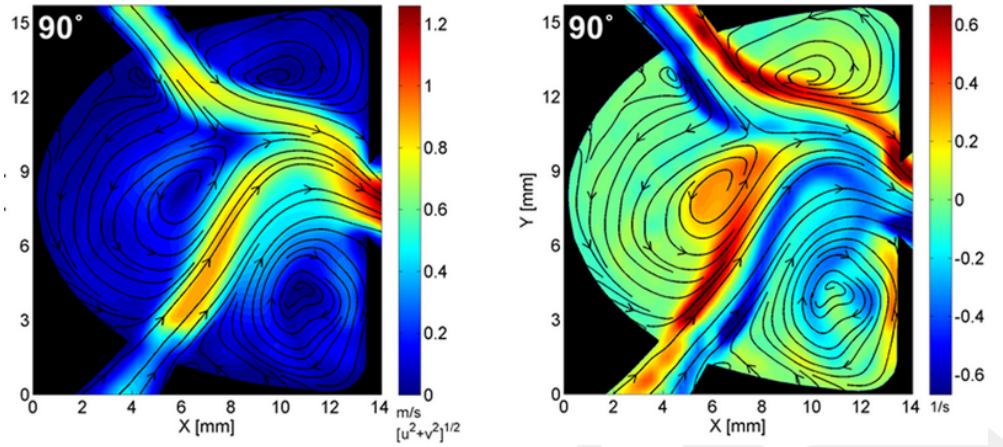

FIG. 10: Same as Fig. 8, but for 90° phase angle.

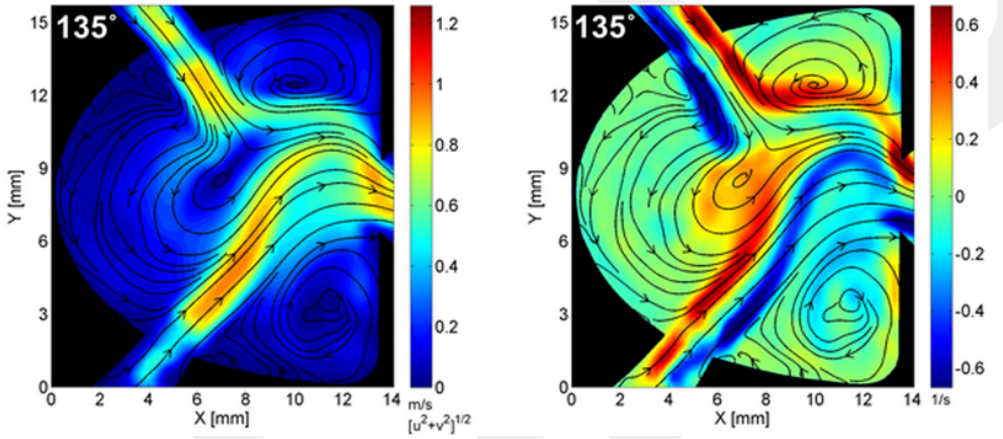

FIG. 11: Same as Fig. 8, but for 135° phase angle.

For the phase angle of 180°, shown in Fig. 12, the results are simply the mirrored images of the results presented at the beginning of the oscillation period. This time the upper jet is cut, while the lower jet energizes the upper-side vortex before its core connects with the exiting jet and the upper-dome vortex is formed by the upper-jet left shear layer. Note that, for this instant, the lower-jet left shear layer energizes the upper-side vortex and the lower-jet right shear layer energizes the lower-side vortex. Furthermore, in the transition regime, side and dome vortices were observed to be stronger than the vortices created in the low–flow rate regime, and consequently, the strength of the vorticity created over the walls has also increased.

The latter half of the oscillation cycle displays a similar mechanism to that just described. As seen in Fig. 13, the upper-dome vortex grows and pushes the upper jet toward the exit while constricting the left branch of the upper jet. The lower-jet potential core

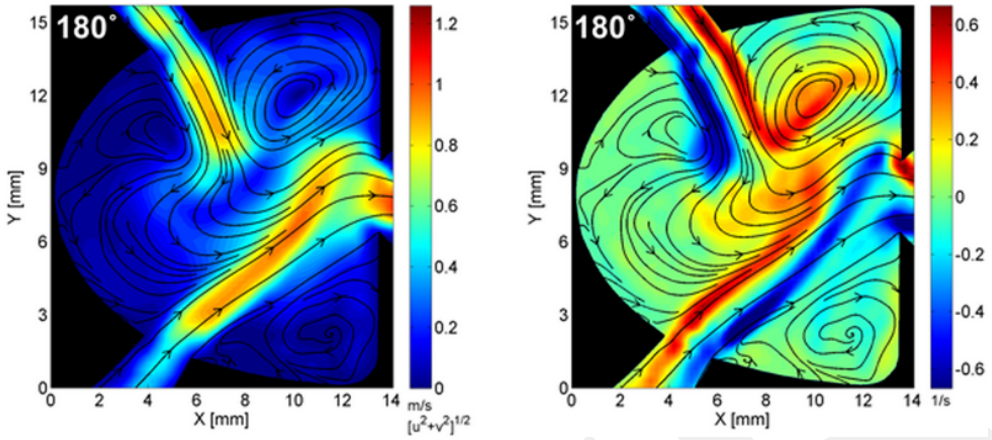

FIG. 12: Same as Fig. 8, but for 180° phase angle.

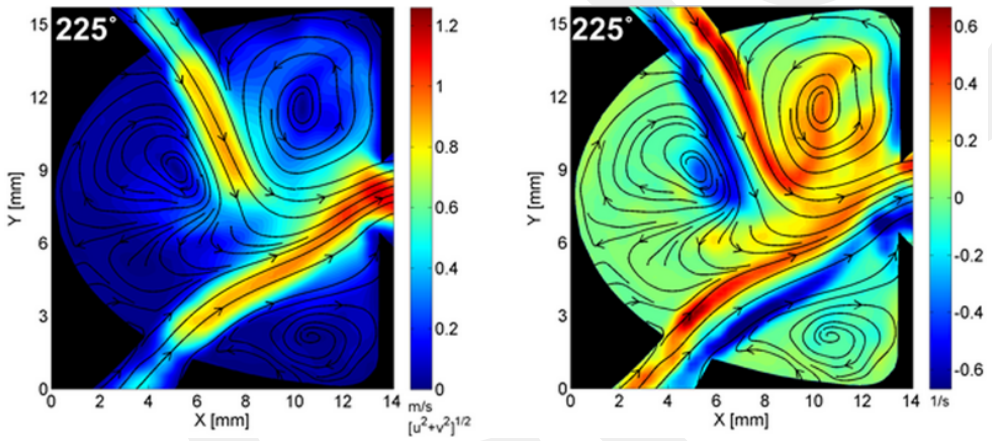

FIG. 13: Same as Fig. 8, but for 225° phase angle.

is connected to the exiting jet at this instant. Figure 14 shows the contours of velocity and vorticity before the dome vortex–saddle point collision. In Fig. 15, which displays results for a phase angle of 351°, the saddle point collision has already occurred and has completely cut the connection of the lower jet's potential core with the exiting jet.

4. CONCLUSION

Details of internal flow physics and the oscillation mechanism of a feedback-free-type fluidic oscillator spray in the transition regime at Re of 1680 were extracted by using a refractive index–matched PIV technique along with a custom-made microphone-tube sensor configuration and a quarter period–based PIV phase-averaging method. Refractive index–matched PIV results indicated the creation of two side and two dome vortices by

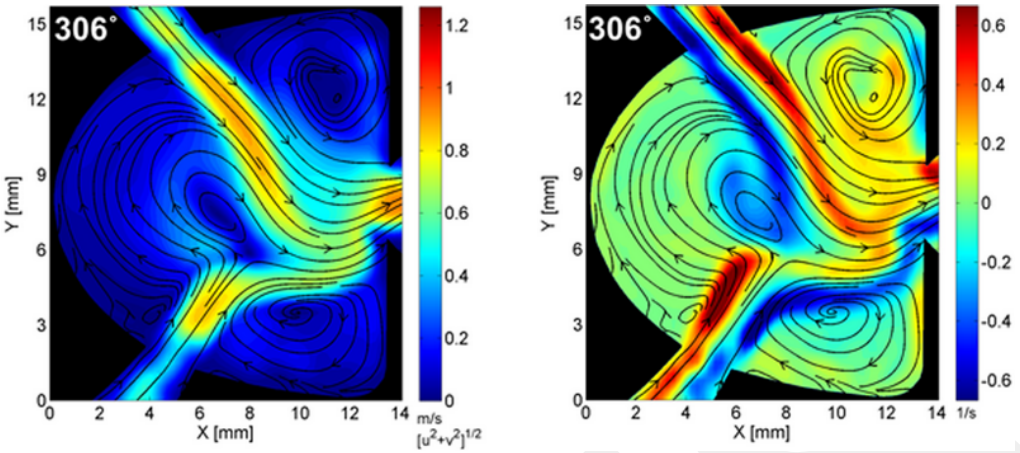

FIG. 14: Same as Fig. 8, but for 306° phase angle.

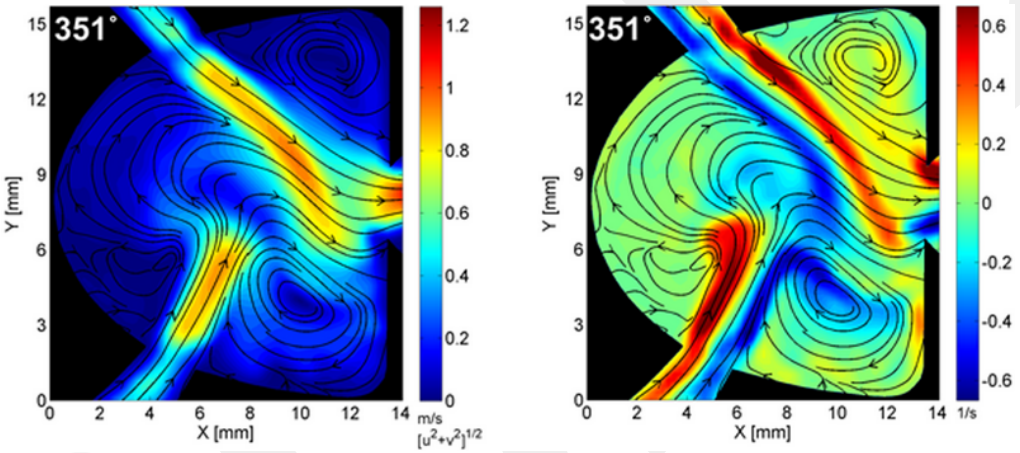

FIG. 15: Same as Fig. 8, but for 351° phase angle.

the shear layers of the jets. Dome vortices were observed to appear and vanish throughout the period and are mainly responsible for the jet bifurcation and kinetic energy transfer. Persistent side vortices trigger the creation of the dome vortices as they change their size, shape, and strength continuously. As the jet is bifurcated by a dome vortex, its connection with the exiting jet weakens. This connecting portion is deflected by the opposing jet, causing the exiting jet's flow direction to alter continuously until the jet connection is cut completely with the exiting jet. Also in the transition regime, the side vortices (lower side and upper side) are periodically energized by the opposite jet in addition to the shear layer that is already energizing them—unlike the low–flow rate regime, in which most of the kinetic energy transferred to the side vortices was acquired from the corresponding shear layer of the nearest jet.

Oscillatory behavior in the transition regime is a consequence of many interesting flow physics features, such as jet collisions, interactions, bifurcations, cutting and bending, and vortex–shear layer and vortex–wall interactions. In contrast to the oscillation mechanism in the low–flow rate regime, each jet's connection with the exiting jet is completely cut by the dome vortex in every period, and the kinetic energy of the bifurcated jet is transferred to the jet that creates the dome vortex. This kinetic energy transfer mechanism overrides the fact that the flow rates of the jets are equal and there would otherwise be no reason for a single input jet to make up the entirety of the exit jet.

REFERENCES

Bidadi, S., Heister, S. D., and Matsutomi, Y., Computational and experimental study of jet interaction fluidic injectors, *Atomization and Sprays*, vol. **21**, no. 2, pp. 127–138, 2011.

Bobusch, B. C., Woszidlo, R., Bergada, J. M., Nayeri, C. N., and Paschereit, C. O., Experimental study of the internal flow structures inside a fluidic oscillator, *Exp. Fluids*, vol. **54**, pp. 1–12, 2013.

Bobusch, B. C., Berndt, P., Paschereit, C. O., and Klein, R., Investigation of fluidic devices for mixing enhancement for the shockless explosion combustion process, *Notes Numer. Fluid Mech. Multidisciplinary Des.*, vol. **127**, pp. 281–297, 2015.

Booth, W. A., Performance evaluation of a high-pressure-recovery bistable fluid amplifier, fluid jet control devices, *Proc. Symp. Fluid Jet Control Devices*, ASME, 1962.

Denshchikov, V. A., Kondrat'ev, V. N., and Romashov, A. N., Interaction between two opposed jets, *Fluid Dyn.*, vol. **13**, no. 6, pp. 924–926, 1978.

Denshchikov, V. A., Kondrat'ev, V. N., Romashov, A. N., and Chubarov, V. M., Auto-oscillations of planar colliding jets, *Fluid Dyn.*, vol. **18**, no. 3, pp. 460–462, 1983.

Gaylord, W. and Carter, V., *Fluerics 27: Flueric Temperature-Sensing Oscillator Design*, report HDL TR-1428, Washington, DC: Harry Diamond Laboratories, 1969.

Gregory, J. W. and Tomac, M. N., A review of fluidic oscillator development and application for flow control, *43rd AIAA Fluid Dynamics Conf. and Exhibit*, AIAA 2013-2474, 2013.

Gregory, J. W., Sullivan, J. P., and Raghu, S., Visualization of jet mixing in a fluidic oscillator, *J. Visual.*, vol. **8**, no. 2, pp. 169–176, 2005.

Gregory, J. W., Sullivan, J. P., Raman, G., and Raghu, S., Characterization of the microfluidic oscillator, *AIAA J.*, vol. **45**, no. 3, pp. 568–576, 2007.

Guyot, D., Paschereit, C. O., and Raghu, S., Active combustion control using a fluidic oscillator for asymmetric fuel flow modulation, *Int. J. Flow Control*, vol. **1**, pp. 155–166, 2009.

Hassaballa, M. and Ziada, S., Self-excited oscillations of two opposing planar air jets, *Phys. Fluids*, vol. **27**, 014109, 2015.

Lush, P. A., A Theoretical and experimental investigation of the switching mechanism in a wall attachment fluid amplifier, *Proc. IFAC Symp. on Fluidics*, 1968.

Meier, E. and Heister, S. D., Computational characterization of the feedback free fluidic oscillator, *50th AIAA/ASME/SAE/ASEE Joint Propulsion Conf.*, AIAA 6.2014-3583, 2014.

Nomoto, A., Yamamoto, K., and Ohshio, Y., Axial impingement of two bounded jets, *Proc. 2nd Int. JSME Symp. on Fluid Machinery and Fluidics*, 1972.

Pawlowski, R. P., Salinger, A. G., Shadid, J. N., and Mountziaris, T. J., Bifurcation and stability analysis of laminar isothermal counter flowing jets, *J. Fluid Mech.*, vol. **551**, pp. 117–139, 2006.

Raghu, S., Feedback-free fluidic oscillator and method, U.S. Patent 6,253,782, July 3, 2001.

Raghu, S., Fluidic oscillators for flow control, *Exp. Fluids*, vol. **54**, pp. 1–11, 2013.

Raman, G., Raghu, S., and Bencic, T. J., Cavity resonance suppression using miniature fluidic oscillators, *5th AIAA Aeroacoustics Conf.*, 1999.

Rolon, J. C., Veynante, D., and Martin, J. P., Counter jet stagnation flows, *Exp. Fluids*, vol. **11**, pp. 313–324, 1991.

Spyropoulos, C. E., Sonic oscillator, *Proc. Fluid Amplification Symp.*, vol. **3**, pp. 27–51, 1964.

Tesař, V. and Bandalusena, H. C. H., Bistable diverter valve in microfluidics, *Exp. Fluids*, vol. **50**, pp. 1225–1233, 2011.

Tesař, V., Zhong, S., and Rasheed, F., New fluidic-oscillator concept for flow-separation control, *AIAA J.*, vol. **51**, no. 2, pp. 397–405, 2013.

Tomac, M. N., *Internal fluid dynamics and frequency characteristics of feedback-free fluidic oscillators*, PhD thesis, The Ohio State University, 2013.

Tomac, M. N. and Gregory, J. W., Frequency studies and scaling effects of jet interaction in a feedback-free fluidic oscillator, *Proc. 50th AIAA Aerospace Sciences Meeting*, AIAA 2012-1248, 2012.

Tomac, M. N. and Gregory, J. W., Jet Interactions in a feedback-free fluidic oscillator at low flow rate region, *43rd AIAA Fluid Dynamics Conf. and Exhibit*, AIAA 2013-2478, 2013.

Tomac, M. N. and Gregory, J. W., Internal jet interaction in a fluidic oscillator at low flow rate, *Exp. Fluids*, vol. **55**, pp. 1–14, 2014.

Warren, R. W. and Peperone, S. J., Fluid amplifications. 1. Basic principles, report TR-1039, Diamond Ordnance Fuze Labs, 1962.